Nafion/silicon oxide

by Mahreni Mahreni

Nafion/silicon oxide/phosphotungstic acid nanocomposite membrane with enhanced proton conductivity

A. Mahreni[a], A.B. Mohamad[a,*], A.A.H. Kadhum[a], W.R.W. Daud[a], S.E. Iyuke[b]

[a] Department of Chemical and Process Engineering, University Kebangsaan Malaysia, 43600, M Bangi, Selangor DE, Malaysia
[b] School of Chemical and Metallurgical Engineering, University of the Witwatersrand, P/Bag 3, Wits 2050, Johannesburg, South Africa

ABSTRACT

Nafion-silicon oxide (SiO_2)-phosphotungstic acid (PWA) composite membrane has been synthesized to improve Nafion based proton exchange membrane fuel cell (PEMFC) performance. The objective of the study is to fabricate Nafion-SiO_2-PWA nanocomposite membrane using sol–gel reaction. The composite is composed of the mixture of Nafion solution, tetra ethoxy orthosilane (TEOS) and PWA solution. The mixed solution was casted at certain temperature until transparent membrane is obtained. Peaks of SiO_2 and PWA in the infrared spectra revealed that both inorganic and organic components are present in the modified Nafion based nanocomposite membrane. Analysis with fuel cell test station showed that higher current density was produced by nanocomposite membrane ($82\,mA\,cm^{-2}$ at $0.6\,V$ for NS15W) than with the Nafion membrane ($30\,mA\,cm^{-2}$ at $0.2\,V$) at $90\,°C$ and 40% relative humidity. The internal resistance was seen to increase with the inorganic content. The internal resistances of the commercial Nafion (N112), NS10W, NS15W and NS20W are 6.33, 4.84, 1.33 and $3.6\,\Omega\,cm^2$, respectively and their Tafel constants are 93.4, 84.4, 11.25 and $26.6\,mV$, respectively. While the nanocomposite membrane results were shown to be better than the commercial Nafion, the overall performances are comparable to those in the open literature.
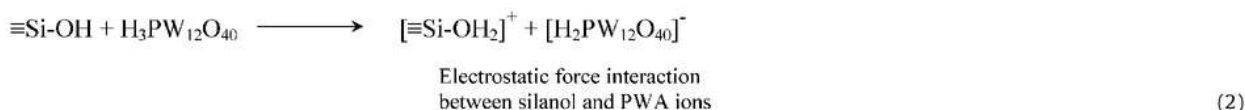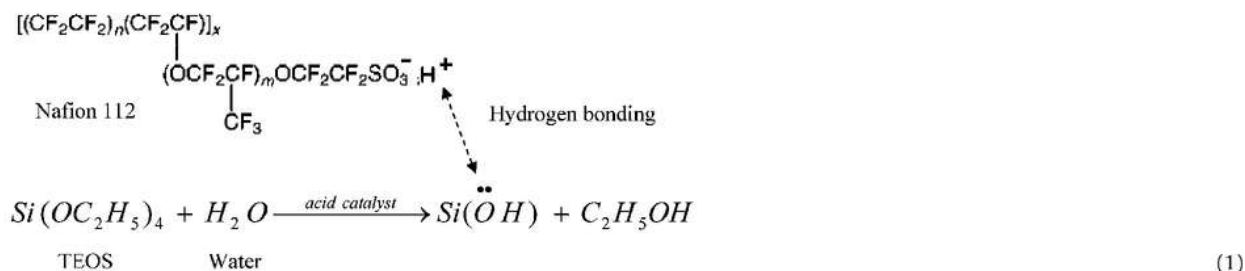
1. Introduction

Perfluorosulfonic acid (PFSA) membranes (e.g. Nafion) are the most widely used polyelectrolyte in polymer electrolyte membrane fuel cells (PEMFCs), because they exhibit excellent properties up to about $90\,°C$ in terms of proton conductivity, mechanical stability and chemical inertia. Moreover, the conductivity of PFSA membranes at low relative humidity (RH) is not sufficient for the fuel cell applications requiring high current densities, while at temperatures above $100\,°C$ and RH close to 100%. This is due to anisotropic membrane swelling that occurs when the membrane is pressed between the electrodes, which provoke irreversible conductivity decay [1]. The possibility to modify physical and chemical properties of a polymer by dispersing inorganic nanopar-

ticles in the polymeric matrix [2–4] encourages the development of proton conducting composite membranes suitable for PEMFCs that could work at temperatures above $100\,°C$. Phosphotungstic acid (PWA), Silicotungstic acid (SiW) and Silicomolibdenic acid (SiMoA) [5], Zirconium phosphate [6], H_3PO_4 [7] have previously been used as fillers in proton conducting polymeric membranes. This is because these materials are proton conductors with good chemical and thermal stability under certain favorable conditions, while the conductivity of PWA is $10^{-2}\,S\,cm^{-1}$ at room temperature [5].

In this study, heteropolyacid (HPA) such as PWA was used as a conductive material additive to modify the Nafion membrane to produce stable composite at moderate temperature and low relative humidity. However, the problem with it is the solubility of PWA that causes leach out from the composite membrane in a polar solvent. PWA is strongly acidic hence they are widely used as solid acids for several acid-catalyzed reactions in liquid phase. Meanwhile, a proposed reaction mechanism between Nafion, SiOH and PWA is presented in Eqs. (1) and (2) [8,9].

* Corresponding author. Tel.: +60 3 892 16406; fax: +60 3 892 16148.
E-mail address: drab@vlsi.eng.ukm.my (A.B. Mohamad).

$$[(CF_2CF_2)_n(CF_2CF)]_x$$

Nafion 112 $(OCF_2CF)_mOCF_2CF_2SO_3^-,H^+$ Hydrogen bonding

CF_3

$$Si(OC_2H_5)_4 + H_2O \xrightarrow{acid\ catalyst} Si(\overset{..}{O}H) + C_2H_5OH \qquad (1)$$

TEOS   Water

$$\equiv Si\text{-}OH + H_3PW_{12}O_{40} \longrightarrow [\equiv Si\text{-}OH_2]^+ + [H_2PW_{12}O_{40}]^- $$

Electrostatic force interaction
between silanol and PWA ions   (2)

Eqs. (1) and (2) suggest that nanocomposite structure of Nafion-SiO$_2$-PWA has strong interaction of hydrogen bonding between Si(OH) and sulfonic acid group from Nafion polymer and electrostatic interaction between Si(OH) and $[H_2PW_{12}O_{40}]^{-1}$ ions. The strong interaction among these components prevents formation of particle aggregate because the bonding among the components takes place at nanoscale or molecular size.

The key parameters that affect the conductivity of the Nafion-SiO$_2$-PWA composite membrane are the particle size of PWA and stability of this particle in the Nafion polymer matrix [5]. The particle size of the additive must be same or less than the ionic cluster size (4–10 nm) in the Nafion membrane matrix. These particles function as proton hopping bridge at the critical condition (low level hydration) of the membrane [5].

Three main synthetic procedures are used to insert HPA particles into the Nafion polymer matrix. The first method is based on the dispersion of pre-formed filler particles in the polymer solution [10]. The second procedure is the "impregnation method", developed by Alberti et al. [1] for cation exchange membranes, which in turn consists of two steps: firstly, the cations of the ionomer are exchanged with Cs cationic species, and then the membrane is impregnated in the PWA solution. A third approach is the sol–gel method, where tetraethoxyorthosilicate (TEOS) solution is used as precursor to immobilize PWA particle using sol–gel reaction. The last method has been used in this study to improve the last two methods and to produce composite from microstructure to nanostructure.

2. Experimental

2.1. Materials

Nafion solution of 5 wt.% (EW 1100 Dupont), TEOS (Si(OC$_2$H$_5$)$_4$) 98%, PWA (H$_3$PW$_{12}$O$_{40}$) 96%, Dimethylformamide (DMF), Sulfuric acid (H$_2$SO$_4$) 98%, Hydrogen Peroxide (H$_2$O$_2$) 30% were all purchased from Aldrich. Deionized water was used as solvent in all experiments.

2.2. Membrane preparation

Appropriately 5 wt.% Nafion solution was evaporated at room temperature to obtain solid Nafion. Solid Nafion was dissolved in DMF solvent to obtain 5 wt.% Nafion solution in DMF. PWA was also dissolved in deionized water and then mixed with TEOS at weight ratio of PWA:SiO$_2$ = 4:10. Subsequently, it was stirred in an ultrasonic bath for 30 min, and added to the Nafion-DMF solution and further stirred in an ultrasonic bath for 6 h. The mixture was allowed to stand at room condition to release trapped air bubbles for another 24 h without

mixing. This solution was casted in a Petri dish and heated at 80 °C for 2 h to remove the solvent. In order to enhance the mechanical properties of the composite matrix, heating was continuously applied at 140 °C at different periods of 2, 4, 6 and 10 h until transparent membrane was obtained. Then, the recast composite membrane was made to detach from the Petri dish by boiling it in the de-ionized water. Finally, the membrane was cleaned by heating at 80 °C in the solution of 3 wt.% H$_2$O$_2$, de-ionized water, 0.5 M H$_2$SO$_4$ and again in de-ionized water until the pH of the washing water becomes almost neutral. These composite membranes are designated NS10W, NS15W and NS20W, whose specifications in ratio of Nafion/TEOS/PWA are 100:10:1.1538; 100:15:1.7303 and 100:20:2.3072 (wt./wt./wt.), respectively, as presented in Table 1.

2.3. Membrane–electrode assembly

Gas diffusion electrodes were fabricated with 20 wt.% Pt on carbon and 0.4 mg Pt cm^{-2}. The membrane was sandwiched between the two electrodes and then hot pressed at 130 °C and 70 atm for 90 s to obtain membrane electrode assembly (MEA).

2.4. Physico-chemical characterization

The morphology of the composite polymer membranes was investigated using the scanning electron microscope (SEM: JEOL-6300F). Before analysis, the membrane was cracked in liquid nitrogen and then sputter coated with fine gold layer after which the micrograph was taken. Energy diffraction X-ray (EDX) was used to analyze elements in the composite membrane. Infrared (IR) attenuated total reflection (ATR) spectra of the composite membranes were measured with Fourier transform infrared (FTIR) spectroscopy (Bio-Rad FTS 6000). UV–vis (UV–vis) spectrometer (LAMBDA 900/10/N102290) in the range of 200–700 nm was used to analyze the absorbance and transmittance of the composite membranes. The transmittance data from the UV–vis and empirical equation approach, which indicated SiO$_2$ as the major constituent. In order to determine the particle diameter of SiO$_2$, the Davis and Mott model (Eqs. (3) and (4)) as reported earlier [11–13] was used to correlate transmittance, absorbance constant, thickness, energy band gap and particle diameter as;

$$T = A\exp(-\alpha d) \qquad (3)$$

where T, A, α and d are transmittance at maximal absorbance ($\lambda_{max.absorbance}$) of N112, NS10W, NS15W and NS20W of the composite membranes, inherent constant, absorbance and thickness of the film, respectively. Using the Davis and Mott model of (Eq. (4)), the energy band gaps of the composite membranes were deter-

Table 1
The composition of the composite membrane solution.

Composite membrane	Composition (g)				
	Nafion	TEOS	SiO_2	PWA	Total weight of Nafion-SiO_2-PWA
NS10W	100	10	2.884	1.1538	104.0378
NS15 (control sample, without W)	100	15	4.325	0	104.325
NS15W	100	15	4.326	1.7303	106.0563
NS20W	100	20	5.768	2.3072	108.0752
NS30W	100	30	8.653	3.4615	112.1145

mined as;

$$\alpha h\upsilon = D(h\upsilon - E_g)^n \qquad (4)$$

where h is Plank constant (6.6×10^{-27} erg s), υ the frequency, E_g the band gap energy (eV) and n is the constant for direct band gap or indirect band gap. E_g is used to determine radius of the particle in the composite membrane by using Eqs. (5) and (6) from other studies [12,13] as;

$$E_{g,nanocrystal} = E_{g,bulk} + \frac{\pi^2 h^{*2}}{2R^2}\left(\frac{1}{m_e} + \frac{1}{m_h}\right) \qquad (5)$$

and

$$h^* = \frac{h}{2\pi} \qquad (6)$$

where $E_{g,nanocrystal}$, $E_{g,bulk}$, h, R, m_e, m_h are the band gap energy of nanocrystal (eV), band gap energy of bulk Si (1.1 eV), Plank's constant, radius of the particle, electron masses ($m_e = 1.08\,m_o$) and hole masses ($m_h = 0.56\,m_o$) of the Si particle. From this equation the radius of the particle in the composite membrane can be determined quantitatively.

Transmission electron microscopy (TEM: JEM-1010 JEOL Electron Microscope). Microtom: *REICHERT ULTRACUTS* Leica was used to determine real particle size in the composite membranes. X-ray diffraction (XRD by Bruker AXS based diffractometer with Cu Kα radiation) analysis has been used to determine the saturated ratio of PWA in the SiO_2 pore and the location of inorganic particles in the polymer matrix as was done by Kukovecz et al. [14].

An important characteristic of the membrane is the water uptake rate (WUR), which provides information on the water retention ability of the membrane. This is calculated from the difference in weight between the wet and dry samples. The wet weight (m_{wet}) was determined after immersion of the samples in water at room temperature for 48 h. As for the dry weight (m_{dry}), the samples were heated in the oven at 120 °C for 2 h. The percentage of water uptake rate is thus given as;

$$WUR = \left(\frac{m_{wet} - m_{dry}}{m_{dry}}\right) \times 100\%. \qquad (7)$$

2.5. Determination of internal resistance, conductivity and cell performance of the composite membranes

The Fuel cell test (FCT) station (FCT-2000 ElectroChem, USA) was used for the cell polarization test and determination of the internal resistance of the membrane. The gas flow of H_2/O_2 was fixed at the stoichiometric ($H_2 + 1/2O_2 \leftrightarrow H_2O$) mole ratio 0.5/0.38 while the hydrogen and oxygen pressures were fixed at 1 atm. The operating temperature of the cell was varied between 30 and 90 °C. The relative humidity was controlled by controlling the water temperature in the H_2 and O_2 gas humidifiers. During the (V–I) measurement, the testing system was stabilized for about 1 h in order to obtain constant value for all the parameters of interest and the resistance of the membranes was measured by optimizing the (V–I) experiments. A mathematical model for polarization curve was used to correlate voltage and current (V–I) at 100 and 40% RH based on a single fuel cell system, which include the flooding parameter as in Eq. (8) [15].

$$E = E_o - b \log(i) - R(i) - \gamma \exp(\omega i) \qquad (8)$$

where E, E_o, b, R, γ and ω are the cell voltage, open circuit voltage, Tafel constant, internal resistance, flooding constant and fitting constant, respectively. The internal resistance of the cell is assumed to be same as the conductivity of the composite membrane. Hence, Eq. (9) was used to calculate the membrane conductivity as;

$$\sigma = \left(\frac{1}{R}\right)\left(\frac{l}{S}\right) \qquad (9)$$

where σ is the conductivity of the composite membrane (S cm^{-1}), R the resistance (ohm), l is thickness of the membrane (cm) and S is contact surface area of the electrode (cm^2) [16,17].

3. Results and discussion

3.1. Characterization of nanosize particles

To determine the presence of PWA particle in the composite membrane, elemental analysis was done using EDX and the result is shown in Fig. 1.

The EDX analysis indicates the presence of C, O, F, S, Si, P, W (elements in Nafion-SiO_2-PWA). Fig. 1 shows EDX analysis of the nanocomposites in which the amount of Si, P and W is varied. EDX studies demonstrated a self-assembly of Si, P and W nanoparticles simultaneously directed on a layer film of polymer via physical and chemical arrangements. Thus, the methodology demonstrated in this study can be a good example of how different types of functional nanometer-sized building blocks can be organized in specific arrangements by physical and chemical self-assembling procedures on structured templates.

Fig. 1 shows clearly that N112 (Nafion) membrane consists of C, F, O and S elements, while NS10W (Fig. 1b) shows a new peak of Si (silica), P (phosphor) and W (tungsten) atoms, as well as in NS15W and NS20W as depicted by Fig. 1c and d, respectively. The new peaks are the reflection of the presence of Si, P and W components in the composite membranes, which are evident that inorganic components that were added to the Nafion solution was fixed in the Nafion polymer network and stable even after washing in the base and acid solutions.

Using the data presented in Fig. 1, the ratio of Si and W in the composite membrane was calculated and the result were shown in Table 2. Table 2 shows the wt.% of Si and W in the solution and in the composite membrane.

Weight ratio of W in the composite membrane that are in the NS10W, NS15W and NS20W are 0.023, 0.07 and 0.17 wt.%, and silica component consist 0.15, 1.04 and 2.64 wt.%. By comparing the wt.% of the W and Si component in the solution and in the composite membrane after post treatment (Table 2), proves that the silica and tungsten particles were stable in the Nafion polymer matrix after post treatment. It can be seen that the wt.% of Si and W in the
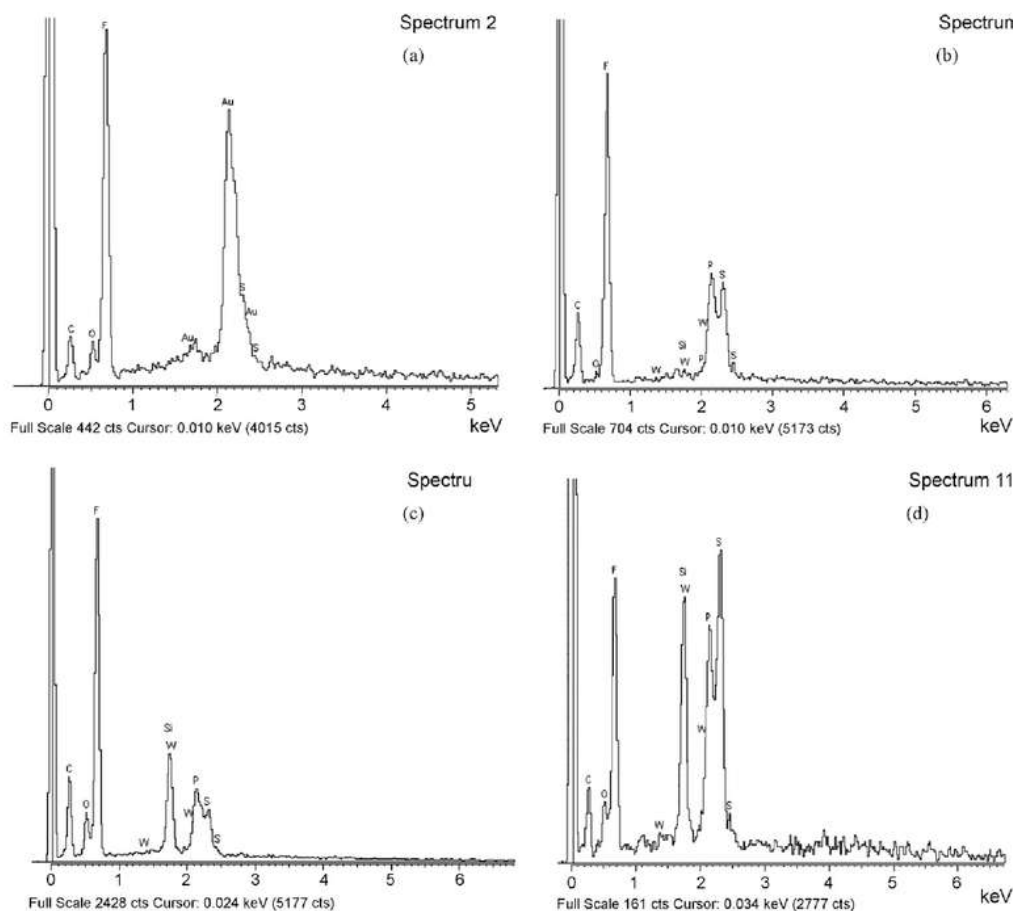
Fig. 1. EDX pattern of (a) N112, (b) NS10W, (c) NS15W and (d) NS20W composite membrane.

NS10 and NS15W in the solution are higher than in the composite membrane. The reduction of element content between solution and composite may be due to leaching of Si and W during post treatment. Reverse phenomena occur with NS20W, where the wt.% of Si and W in the solution was less than in the composite membrane. The reason may be the conversion of SiOH molecule to SiO_2 in the NS20W membrane during condensation reaction meaning, that SiOH molecules were present besides SiO_2, while H component in the SiOH molecules could increase the ratio of Si. Note the H atom could not be detected due to the amount of the component that was less than 0.01 wt.% in the mixture, such that the peak reflection of H component did not appear in the EDX pattern. The wt.% of W atom in the solution is less than in the membrane film, because the crystal water of PWA ($H_3PW_{12}O_{40} \cdot xH_2O$) molecule in the NS20W membrane increased in wt. percent.

To determine the real nanoparticle size of Si and PWA, the TEM analysis is used, and the results are shown in Fig. 2, where the presence of inorganic (Si and PWA) nanoparticles is clearly observed.

As shown in Fig. 2 the average particle diameters for the inorganic compounds (Si and PWA) in the composites are 6.9, 7.864 and 12.641 nm for NS10W, NS15W and NS20W, respectively. The particle dispersion is more obvious on the polymer surface for NS10W and NS15W when compared with NS20W where bigger nanoparticle agglomerates are apparent. This could suggest that the PWA particles are located on the surface of the polymer. The TEM analysis presents a more homogenous particle distribution for NS10W and NS15W where SiO_2 and PWA particle sizes are less than Nafion cluster and that these particles are located in the Nafion cluster. In other words, it may be explained that the SiO_2 and PWA particles in NS10W and NS15W composite membranes are entrapped in the Nafion cluster and therefore may possess higher conductivity if compared with the composite of NS20W that had bigger particle distribution on the surface of the Nafion membrane. XRD analysis has been done to indicate the location of the particle in the composite membrane. Fig. 3 shows XRD pattern of pure SiO_2 (1), PWA particle (2), NS20W (3). NS15W (4), NS10W (5) and N112 (6).

The X-ray diffraction pattern of pure SiO_2 (Fig. 3) (1) showed small peak of 2θ values, whose analysis supports the semi-crystalline nature of SiO_2 [19]. The X-ray diffraction pattern of pure

Table 2
Comparison of Si and W content in the solution and in the composite membrane.

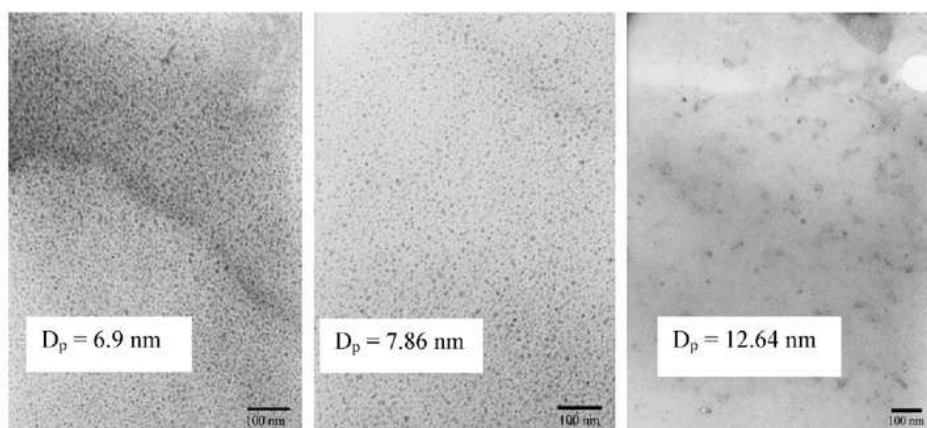| Membrane	wt.% Si in the solution	wt.% Si in the composite membrane	wt.% W in solution	wt.% W in the composite membrane
NS10W	1.29	0.15	0.07	0.023
NS15W	1.90	1.04	0.10	0.07
NS20W	2.48	2.64	0.13	0.17

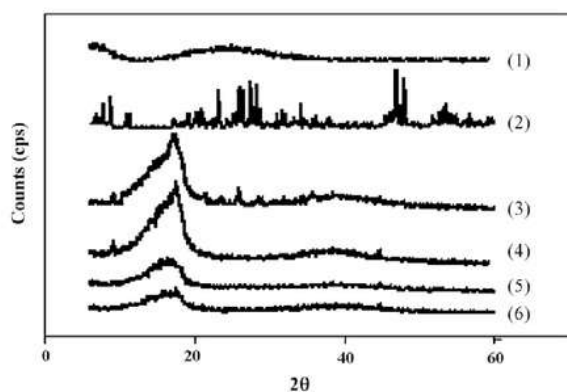**Fig. 2.** TEM images of NS10, NS15 and NS20W composite membrane.

Fig. 3. XRD pattern of (1) pure SiO2, (2) pure PWA, (3) NS20W, (4) NS15W, (5) NS10W and (6) N112 membrane.

PWA (Fig. 3) (2) showed large peak of 2θ values that supports its crystalline nature. The XRD pattern of specimen (NS20W) prepared by sol–gel process clearly showed that sample (3) (NS20W) membrane has reflection due to crystalline PWA on the surface. The smaller the PWA loading the less reflection in the pattern. For the sample having only 1.15 wt.% PWA (NS10W) no clear reflection was found. This behavior suggests that PWA particles are present in this sample in molecular size distribution or in very small clusters undetectable by XRD [14].

3.2. Microstructure of the composite membrane

The morphology of the composite Nafion-SiO$_2$-PWA recasted membranes is shown in Fig. 4. It can be seen that the solid SiO$_2$ and PWA are uniformly distributed within the membrane and do not form any agglomerate structures. The SiO$_2$ and PWA particles are observed to be in the range of 6–12 nm while the thickness of composite membrane is measured to be 70 ± 5 μm.

3.3. Clarity analysis

The time required to produce transparent membrane is 10 h at temperature of 140 °C for each of the composite membrane (NS10W, NS15W and NS20W). After post treatment of washing and drying, the membrane was analyzed using UV–vis method to determine qualitatively the amount of inorganic phase distribution in the organic polymer matrix. The transparency of the composite membrane is a measure of inorganic phase distribution in the range of nanoscale dimension in the organic polymer matrix [18]. If phase dissociation took place, the composite membrane formed is neither transparent nor translucent. Phase separation and homogeneity of the particle distribution also influence the mechanical strength properties of the membrane. Physical visibility of Nafion 112 (commercial), NS10W, NS15 (without PWA in the composite), NS15W, NS20W and NS30W membranes are presented in Table 3. It shows that all the composite membranes are transparent in the UV–vis spectrum, which indicated the absence of the phase dissociation of both the inorganic and organic phases.
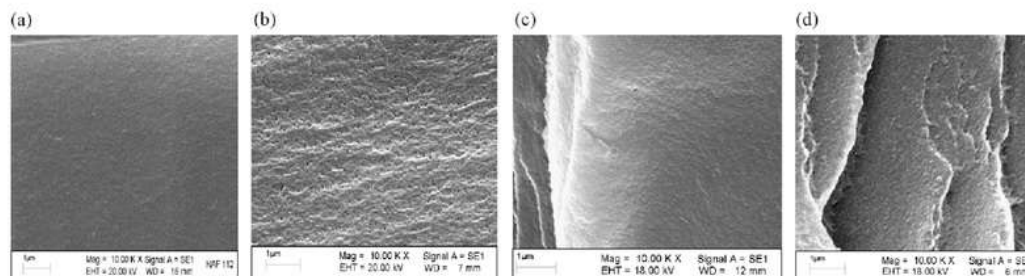

Fig. 4. Cross section of SEM images (a) Nafion 112 (commercial), (b) NS10W, (c) NS15W and (d) NS20W.

Table 3
Clarity of N112, NS10W, NS15W and NS20W.

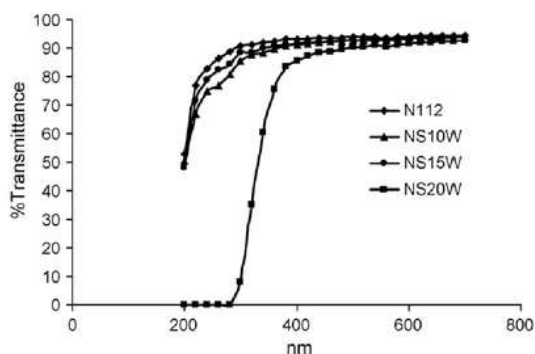| Composite membrane	Clarity	Surface properties
N112	Transparent	Homogeneous
NS15	Transparent	Homogeneous
NS10W	Transparent	Homogeneous
NS15W	Transparent	Homogeneous
NS20W	Transparent	Homogeneous
NS30W	Transparent	Crack

Fig. 5. Transmittance versus wavelength (λ) at 200–700 nm of the N112, NS10W, NS15W and NS20W membranes.

The results also show that there is chemical interaction between the organic and inorganic compounds through the hydrogen bonding between the sulfonate group of Nafion polymer and hydroxyl (OH) group of the silanol Si(OH) that was produced via the hydrolysis of TEOS molecules. On the other hand, the electrostatic interactions between the ions of $H_3PW_{12}O_{40}$ and Si(OH) took place in the composite membrane material. Therefore, the composite material has strong bonding between organic and inorganic compounds, which could have been responsible for the homogeneous distribution of the inorganic phase in the organic matrix.

UV–vis spectra of N112, NS10W, NS15W and NS20W membranes are shown in Fig. 5. The figure shows high inorganic content in the organic matrix with the transmittances of all the membranes

above 90% at the wavelength of 700 nm. High transmittance of the composite membranes indicates that inorganic particles within the ionic clusters are in nanosize dimension [18]. The result of UV–vis analysis for all the membranes are presented in Fig. 5, which showed that N112, NS10W, NS15W membranes have maximal absorbance at wavelength of 250 nm, while NS20W has its maximal absorbance at 400 nm. The transmittances of N112, NS10W and NS15W at 200 nm wavelength are 53, 51 and 48%, respectively. Using these values in Eq. (3), with $A = 1$ and the thickness of the membrane to be 70 μm, the absorbance constant for each of the membranes can be determined.

The band gap energy for every membrane was determined using Eq. (4) with the plot of $(\alpha h\nu)^2$ versus $h\nu$ giving non-linear relationship as shown in Fig. 6. The extrapolation of the curve in the linear region to $(\alpha h\nu)^2 = 0$ axis gives the value of band gap (E_g) of the material. The plot of $(\alpha h\nu)^2$ versus $h\nu$ is shown in Fig. 6a for NS20W membrane and in Fig. 6b for N112, NS10W and NS15W membranes. Extrapolation of Fig. 6b gave the energy band gap for the membranes (Table 4), which are comparable with the particle band gap energy in bulk condition as was reported in the earlier studies [20,21]. In order to determine particle size of SiO_2 in the composite membrane, Eq. (5) was used with the values for $E_{g,nanocrystal}$ and $E_{g,bulk}$ as presented in Table 4.

Table 4 shows that if the inorganic content increases, the band gap energy of the composite membrane would be reduced while the particle diameter increases. This phenomenon reveals that higher inorganic content in the composite membrane increases the particle size due to the high concentration of the particle to form aggregate [21].

3.4. Membrane hydration

As mentioned above, the hydration of the membrane is closely related to its conductivity and the mechanical stability [22,23], hence the hydration of the membrane could also be measured by water uptake method as expressed above in Eq. (7). The variations of the water uptake of the inorganically modified membranes with that of the commercial Nafion 112 have been shown in Fig. 5. It is observed that the composite membranes have the tendency to absorb more water than the commercial membrane sample, which
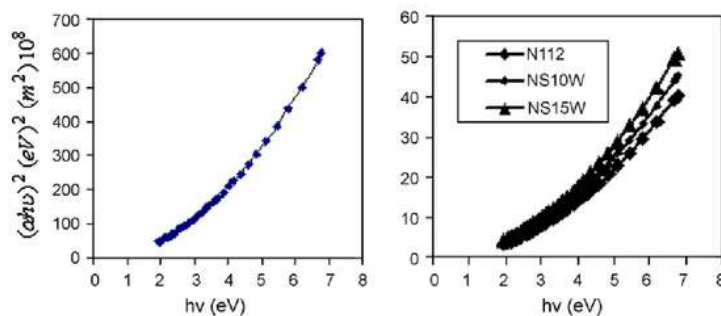
Fig. 6. Plot of $(\alpha h\nu)^2$ versus $h\nu$ (a) NS20W (b) N112, NS10W and NS15W.

Table 4
Comparison of energy band gap of the SiO_2 composite.

Membrane	This study			Garrido et al. [19]	
	E_g (eV)	Particle diameter from UV–vis (nm)	Particle diameter from TEM (nm)	E_g (eV)	Particle diameter (nm)
NS10W	2.75	4.72	6.69	2.3	2.1
NS15W	2.5	5.13	7.864	2.11	3
NS20W	2.4	5.32	12.641	1.5	6

Table 5
Water uptake rate of the membranes.

Membrane	Composition	Water uptake rate (g water/g membrane) $\times$ 100 %
N112	Nafion	26.52
NS10W	Nafion-SiO$_2$-PWA	30.25
NS15	Nafion-SiO$_2$	30.01
NS15W	Nafion-SiO$_2$-PWA	33.43
NS20W	Nafion-SiO$_2$-PWA	32.72
NS30W	Nafion-SiO$_2$-PWA	31.96

is consistent with the work of others [23]. The water uptake characteristic of the Nafion-SiO$_2$-PWA composite membrane is found to be improved from that of the pure Nafion membrane. The water uptake of the Nafion recast membrane is also increased when the HPA is increased. These results can be supported from the fact that the hydrophilic characters of the SiO$_2$ and PWA play a dominant role in the increase water uptake rate of the composite membrane. The percentages of water uptake rate presented in Table 5 for Nafion 112, NS10W, NS15, NS15W and NS20W membranes are 26.52, 30.25, 30.01, 33.43 and 32.72 and 31.96 (wt. % water/wt. membrane), respectively.

The WUR value increased with the increase of the SiO$_2$ and PWA content in the composite membrane of up to TEOS/Nafion ratio of 15/100, while above this ratio, the WUR decreased. Water uptake rate is related to the basic membrane properties and plays an essential role in the membrane behavior. Proton conductivity across the membrane depends to large extend on the amount and behavior of water that can be absorbed by the membrane. Water may influence the ionomer microstructure, creating clusters and altering channel sizes, thus involved in modifying the mechanical properties. The increase in water uptake rate can be attributed to the water retention of the incorporated silica due to hydrogen bonding occurring between SiOH groups and water crystal of PWA particle in the composite membrane. As shown in Table 5, the role of PWA particles in the WUR is displayed by the fact that WUR of NS15 (without PWA in the composite) (30.01 wt. % water/wt. membrane) is less than WUR of NS15W (33.43 g water/g membrane). This implies that the PWA in the membrane has increased the water uptake rate.

Table 5 showed that the water uptake increased from 30.25 (NS10W) to 33.43% (NS15W) and then dropped to 32.72% as the TEOS/Nafion ratio increases from 10/100 to 20/100. This might be due to the decrease in the water affinity of the composite membrane at the PWA/Nafion ratio greater than 1.8/100. At this PWA/Nafion ratio, the composite has large particle size such that it could not get into the ionic cluster of the Nafion membrane. In accordance with the proton hopping model mentioned above, the effective addition of PWA is related to its role in increasing the conductivity of the Nafion membrane at high temperature and low relative humidity. The conductivity increases if the particle is incorporated into the cluster of Nafion membrane because in the ionic cluster the particles act as proton hopping bridge of the proton transfer [1]. For NS10W and NS15W the particle sizes are small enough to be occupied within the ionic cluster and its role as proton hopping bridge of the proton transfer at dry condition can be reached. This is appropriate with the nature of the PWA and SiO$_2$ as hygroscopic materials that can introduce water crystal into the ionic cluster. For NS20W with diameter particle size larger than the cluster size, the PWA can be assumed to be adsorbed on the outside of the cluster. Such water molecules outside the cluster have physical bonding, which is easily released during heat treatment of the membrane. So the contribution of the particle to water uptake rate in this composite membrane is not apparent if the PWA particle on the ionic cluster cannot be used as proton hopping bridge at low level of hydration of the membrane. Under this condition, the

water will be released from the membrane during heat treatment thus resulting into a dry membrane.

3.5. FTIR analysis

Fourier Transform Infrared spectra at wave numbers 4000–400 cm^{-1} for the composite membranes have been recorded and analyzed. The spectra indicated peak shifts in the composite membranes due to the change in the inorganic moiety content. They also show that the particle sizes of PWA and SiO$_2$ at nano dimension have undergone chemical interactions between the sulfonate group and SiO$_2$ of PWA. IR spectra for all the composite membranes are presented in Fig. 7a–c. Fig. 7b shows that vibration of C–O–C bonding at NS10W composite membrane at the wave number 969 cm^{-1} shifts to lower wave number for NS20W (Fig. 7c) membrane and NS15W. This phenomenon can be attributed to the strong interaction of SiO$_2$ component as compared to the side chain of the Nafion polymer of the SiO$_2$ content [5,10,24].

The major vibrational structures associated with the Nafion membrane (Fig. 7a) are found in all three nano-composite membranes. The two C–F stretching vibrations of the PTFE backbone can be observed at 1194 cm^{-1} and 1134 cm^{-1}. The peaks observed at 1054 and 9670 cm^{-1} are attributed to the stretching vibration moieties of SO$_3$$^-$ and C–O–C, respectively. The peak of Si–O–Si is seen at wave number 800 cm^{-1} while the W–O–W stretching vibrations in the composite membrane are observed at wave numbers 755–765 cm^{-1}. The observable peak at 980 cm^{-1} represents the vibration moiety of the W=O functional group. Therefore, it is evident from these data that the SiO$_2$ and PWA are indeed present in the composite membranes even after these membranes had undergone the pretreatment process of washing using 3 wt.% H$_2$O$_2$ and 0.5 M H$_2$SO$_4$ solution at the temperature of 80 °C for 1 h. It is apparent that the SiO$_2$ and PWA are compatible with Nafion membrane and the PWA is able to be immobilized into the SiO$_2$ media. The peak observed at 800 cm^{-1} in the spectrum of Nafion-SiO$_2$–PWA composite membrane with the ratio of TEOS/Nafion-PWA membrane 10/100 (NS10W) is less than that for NS15W and NS20W. Bonding structure of P–O–P of Kegin structure is not apparent in the Infrared spectrum may be due to overlap with asymmetric vibration of CF$_2$ ($_{as,v}$CF$_2$) structure. While P–O (central tetrahedral of Kegin unit) corresponding to the peak at wave numbers (1079–1278) cm^{-1} overlap with symmetric vibration of CF$_2$ ($_{s,v}$CF$_2$). Interaction between organic polymer and inorganic material assigned by shift of the wave number corresponding to the SO$_3$ bonding structure at 1054 cm^{-1} in the N112 shifts to 1055 cm^{-1} in NS10W. The wave number change to higher value in the NS10W composite membrane explains the interaction between SiOH from inorganic component and SO$_3$ from Nafion via hydrogen bonding. While for NS15W and NS20W the wave number shift of SO$_3$ was not observed. The wave number shift may be associated with the rearrangement of molecular or the back bone structure of the nanocomposites due to the interaction between Nafion and the inorganic compounds [2].

3.6. Single cell performance

Performance of the single cell MEA using all the membranes (N112, NS10W, NS15, NS15W and NS20W), was obtained from the cell voltage versus current density measurement. The results of the test at temperature of 90 °C and 40% RH are presented in Fig. 8a–e. All the experimental data are presented together with mathematical correlation based on Eq. (8) above with volumetric velocity of air at 4.15 L/min, volumetric velocity of H$_2$ at 1.15 L/min and total pressure of 1.3 atm. Interestingly, the model shows good fitting correlation with the experimental data for all the membranes under study. The optimized parameters used in fitting the model
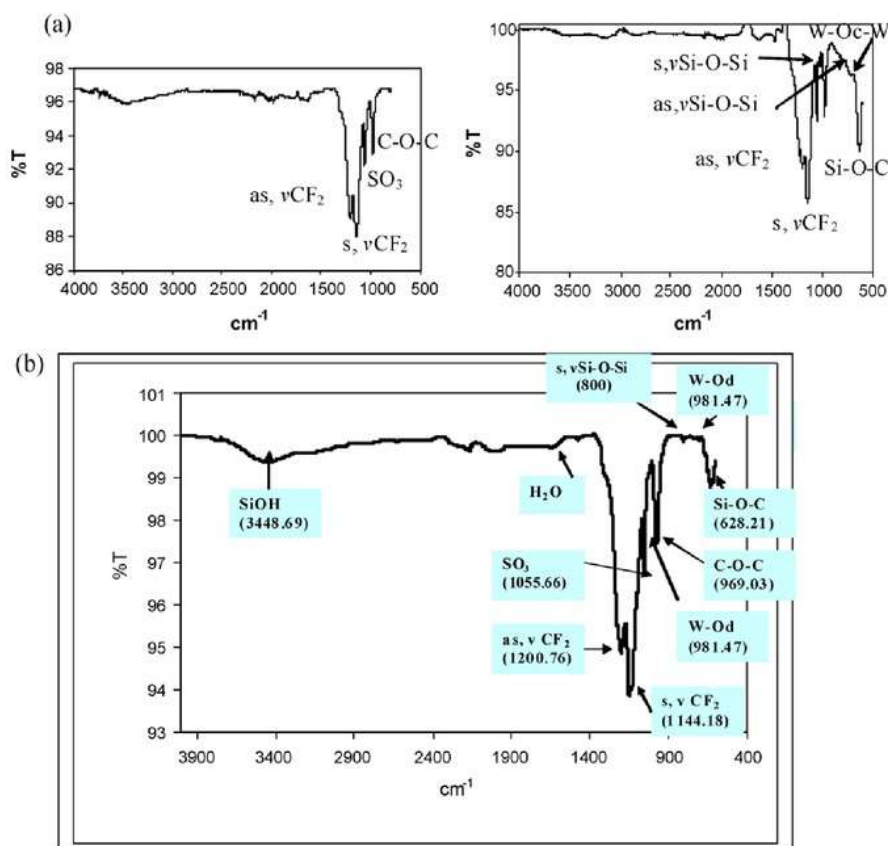
Fig. 7. FTIR spectra (a) N112 commercial membrane, (b) NS10W composite membrane and (c) NS20W composite membrane [NS15W spectrum not shown].

(Eq. (8)) with the experiments for all membranes are presented in Table 6.

In comparing the current density and resistivity of the cell, the order of performance of the composite membranes starting from the best to worst is as follows: NS15W, NS20W, NS10W, NS15, N112. This trend can clearly be rationalized by considering the physico-chemical and electrochemical properties of the membrane as indicated in the SEM, TEM, WUR and UV–vis analyses. The low

water uptake rate observed with NS20W when compared to that of NS15W is perhaps due to the fact that the particle sizes of SiO_2 and PWA are bigger than that of the ionic cluster, such that the inorganic particles were adsorbed on the outer surface of the cluster.

Fig. 8 shows the performance of single cell using N112, NS10W, NS15, NS15W and NS20W as the solid electrolyte operated at 90 °C and 40% RH. The best performance under these conditions was obtained for NS15W, which produced current density of $82\,mA\,cm^{-2}$ at 0.6 V as compared to the Nafion membrane with $30\,mA\,cm^{-2}$ at 0.2 V. All other composite membranes (NS20W, NS10W and NS15) showed better performance than the Nafion membrane under these conditions possibly due to the incorporation of the inorganic hygroscopic materials to the Nafion polymer matrix.
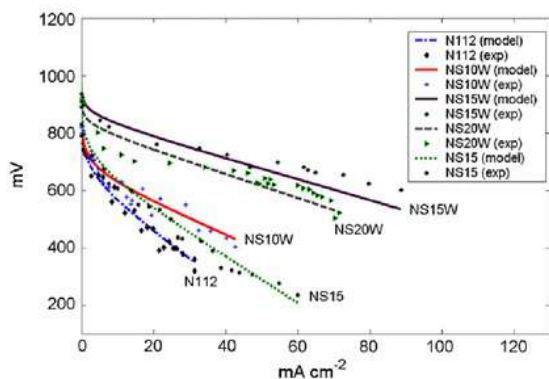

Fig. 8. Polarization curves of N112, NS10W, NS15W, NS20W and NS15 membranes at 90 °C and 40% RH.

Table 6
Open circuit voltage, Tafel slope, internal resistance, flooding constants and fitting constant for N112, NS10W, NS15W and NS20W membranes, with thickness 70 μm and surface area 50 cm².

Membrane	E_o (mV)	b (mV)	R ($\Omega\,cm^2$)	γ (mV) ($\omega = 0.01$)	Proton conductivity ($\times 10^3\,S\,cm^{-1}$)
N112	895.40	43.40	6.01	150.60	1.16
NS10W	890.91	35.59	2.79	135.57	2.51
NS15	890.87	42.765	5.84	85.987	1.19
NS15W	935.87	18.40	2.45	30.00	2.85
NS20W	912.49	16.55	3.01	49.66	2.32

3.7. The physics behind the improvement in nanocomposite performance

The proton exchange membranes (PEM) inherently contain certain amount of structural water, which exists as chemically adsorbed water, crystal water or some forms of chemical groups containing hydrogen bonding which are strongly connected with the structure. The amount of physically adsorbed water changes reversibly with the vapor pressure in the gas phase at a given temperature, while chemically adsorbed water is caused by the chemical force between the water molecules and the sulfonic group that exist at the end of side chain of Nafion polymer. Thus the amount of chemically absorbed water cannot be desorbed at the same temperature as it is adsorbed. In other words heating is required to desorb chemically absorbed water. Accordingly, since the amount of structural water does not change with vapor pressure or temperature, the amount of structural water cannot be quantified by the adsorption method of water vapor [25]. Therefore, incorporated inorganic compound like PWA that is hygroscopic and has high proton conductivity properties in the Nafion cluster strongly increase the amount of structural water in the film. In this case, the role of inorganic compound in the Nafion cluster is thus to create capillary condensation phenomena in the polymer matrix, which condenses water molecules in the pore network at pressure less than saturated favor pressure [26]. Hence, the membrane is not dry at low relative humidity and conductivity is not reduced dramatically in low relative humidity condition as well.

4. Conclusions

The sol–gel method has been used to improve the structure of Nafion/SiO$_2$/PWA composite membrane from micro composite to nano-composite. Particle diameters of SiO$_2$ and PWA in the composite membranes of NS10W, NS15W and NS20W with 2.1, 3 and 6 nm, respectively, has been obtained at annealing temperature of 140 °C in 10 h. It can be concluded that SiO$_2$ particle was incorporated into the ionic cluster network of Nafion polymer matrix. Physico-chemical characterization was used to compare the composites with pure Nafion membrane and observed that water uptake rate increases with SiO$_2$ and PWA content in the composites. At TEOS/Nafion ratio of 15/100, the water uptake was 33.43 wt.% water/wt. membrane while at the ratio of 20/100 the water uptake was reduced to 32.72%. The same trend was observed for the proton conductivity where maximum value was achieved at the TEOS/Nafion ratio of 15/100 (w/w). Fuel cell performance on single cell was shown to be improved for all of the SiO$_2$ and PWA loaded composite membranes as compared to the pure Nafion membrane. This enhanced performance can be attributed to the high conductivity found in these nanocomposite membranes. The nanocomposite membrane NS15W (TEOS/Nafion = 15/100) showed the best fuel cell performance at the cell operational temperature of 90 °C and 40% relative humidity.

Acknowledgement

References

[1] G. Alberti, M. Casciola, D. Capitán, A. Donnadio, R. Narducci, M. Pica, M. Sganappa, Novel Nafion–zirconium phosphate nanocomposite membranes with enhanced stability of proton conductivity at medium temperature and high relative humidity, Electrochim. Acta 52 (2007) 8125.

[2] V. Ramani, H.R. Kunz, J.M. Fenton, Effect of particle size reduction on the conductivity of Nafion/phosphotungstic acid composite membranes, J. Membr. Sci. 266 (2005) 110.

[3] P. Staiti, A.S. Arico, V. Baglio, F. Lufrano, E. Passalacqua, V. Antonucci, Hybrid Nafion-silica membranes doped with heteropolyacids for application in direct methanol fuel cells, Solid State Ionics 145 (2001) 101.

[4] K.T. Ajemian, S. Srinivasan, J. Benziger, A.B. Bocarsly, Investigation of PEMFC operation above 100 C employing perfluorosulfonic acid silicon oxide composite membranes, J. Power Sources 109 (2002) 356.

[5] V. Ramani, H.R. Kunz, F.M. Fenton, Investigation of Nafion/HPA composite membranes for high temperature/low relative humidity PEMFC operation, J. Membr. Sci. 232 (2004) 31.

[6] F. Bauer, M. Willert-Porada, Microstructure characterization of Zr-phosphate-Nafion membrane for direct membrane fuel cell (DMFC) applications, J. Membr. Sci. 233 (2004) 141.

[7] Y. Zhai, H. Zhang, J. Hu, B. Yi, Preparation and characterization of sulfated zirconia (SO$_4^{-2}$/ZrO$_2$/Nafion composite membrane for PEMFC operation at high temperature/low humidity, J. Membr. Sci. 280 (2006) 148.

[8] H.G. Haobold, T.H. Vad, H. Jungbluth, P. Hiller, Nano structure of Nafion a SAXS study, Electrochim. Acta 46 (2001) 1559.

[9] M.H. Bhure, I. Kumar, A.D. Natu, R.C. Chikate, C.V. Rode, Silica with modified acid sites as a solid catalyst for selective cleavage of tert-butyldimethylsilyl ethers, Catal. Commun., in press.

[10] Z.G. Shao, P. Joghee, I.M. Hsing, Preparation and characterization of Hybrid Nafion-silica membrane doped with phosphotungstic acid for high temperature operation of proton exchange membrane fuel cells, J. Membr. Sci. 229 (2004) 43.

[11] M. Aparacio, Y. Castro, A. Duran, Synthesis and characterization of proton conducting styrene-co-methacrylate-silica sol-gel membranes containing tungstophosphoric acid, Solid State Ionics 176 (2005) 333.

[12] K. Singh, N.S. Saxena, O.N. Srivastava, D. Patidar, T.P. Sharma, Energy band gap of Se$_{100-x}$In$_x$ chalcogenide glasses, Chalcogenide Lett. 33 (2006) 363.

[13] H. Xu, H. Li, C. Wu, J. Chu, Y. Yan, H. Shu, Preparation, characterization and photolytic activity of transition metal-loaded BiVO$_4$, Mater. Sci. Eng., B 147 (2008) 52.

[14] A. Kukovecz, Zs Balogi, Z. Konya, M. Toba, P. Lentz, S.-I. Niwa, F. Mizukami, A. Molnar, J.B. Nagy, I. Kiricsi, Synthesis, characterization and catalytic application of sol-gel derived silica-phosphotungstic acid composites, J. Appl. Catal. A: Gen. 228 (2002) 86.

[15] J.J. Baschuk, X. Li, Modelling of polymer electrolyte membrane fuel cells with variable degree of water flooding, J. Power Sources 86 (2000) 181.

[16] T. Sancho, J. Soler, M.P. Pina, Conductivity in zeolite-polymer composite membranes for PEMFCs, J. Power Sources 169 (2007) 92.

[17] W. Jang, S. Choi, S. Lee, Y. Shul, H. Han, Characterizations and stability of polyimideephosphotungstic acid composite electrolyte membranes for fuel cell, Polym. Degrad. Stab. 92 (2007) 1289.

[18] P.K. Khanna, N. Singh, S. Hasan, A.K. Viswanath, Synthesis of Ag/polyaniline nanocomposite via in-situ photo redox mechanism, Mater. Chem. Phys. 92 (2005) 214.

[19] A. Wekar, S.A. Siddiqui, I. Khan, Synthesis, characterization and ion-exchange properties of a new and novel "inorganic-organic" hybrid cation exchanger: poly(methylmethacrylate) Zr(IV) phosphate, Colloids Surf. A: Physicochem. Eng. Aspects 295 (2007) 193.

[20] H.M. Wang, P. Fang, Z. Chen, S. Wang, Synthesis and characterization of CdS/PVA nanocomposite films, J. Surf. Sci. 253 (2007) 8495.

[21] B. Garrido, M. Lopez, P. Rodriguez, C. Garcia, P. Pellegrino, R. Ferre, J.A. Moreno, J.R. Morante, C. Bonafos, M. Carrada, A. Claverie, J. de Latore, A. Souifi, Optical and electrical properties of Si-nanocrystals ion beam synthesized in SiO$_2$, NIM B 216 (2004) 213.

[22] A.C. Sacca, R. Pedicini, G. Portale, L.D. Ilario, A. Longo, A. Mortorana, E. Passalacqua, Structural and electrochemical investigation on re-cast Nafion membranes for polymer electrolyte fuel cells (PEFCs) application 1, J. Membr. Sci. 278 (2005) 105.

[23] R. Jiang, H.R. Kunz, J.M. Fenton, Composite silica/Nafion membrane prepared by tetraethoxyorthosilicate sol-gel reaction and solution casting for DMFC, J. Membr. Sci. 272 (2006) 116.

[24] J.D. Kim, I. Honma, Synthesis and proton conducting properties of Zirconia bridge hydrocarbon/phospotungstic acid hybrid materials, Electrochim. Acta 49 (2004) 3179.

[25] H. Takata, M. Nishikawa, Y. Arimura, T. Egawa, S. Fukada, M. Yoshitake, Study on water uptake of proton exchange membrane by using tritiated water sorption method, Hydrogen Energy 30 (2005) 1017.

[26] F. Celistini, Capillary condensation within nanopores of various geometries, Phys. Lett. A 228 (1997) 84.

Nafion/silicon oxide

4%
SIMILARITY INDEX

%
INTERNET SOURCES

%
PUBLICATIONS

4%
STUDENT PAPERS

PRIMARY SOURCES

1	Submitted to Federal University of Technology Student Paper	2%
2	Submitted to The Chicago School of Professional Psychology Student Paper	2%

Exclude quotes	On	Exclude matches	< 2%
Exclude bibliography	On		